Available online at www.sciencedirect.com

SciVerse ScienceDirect

Ceramics International 38 (2012) 3261–3272

CERAMICS INTERNATIONAL

www.elsevier.com/locate/ceramint

Influence of iron content on the color of the C_3A–Fe_2O_3 system synthesized under different conditions of temperature, atmosphere and cooling

Francisco Vázquez-Acosta [a], Leticia M. Torres-Martínez [a,*], Waltter López-González [b], Jorge Ibarra-Rodríguez [c]

[a] *Universidad Autónoma de Nuevo León, UANL, Facultad de Ingeniería Civil, Instituto de Ingeniería Civil, Departamento de Ecomateriales y Energía, Av. Universidad S/N, San Nicolás de los Garza, Nuevo León, C.P. 66451, Mexico*

[b] *Sika Mexicana S.A. de C.V., Carretera Libre a Celaya Km. 8.5, Fracc. Industrial Balvanera, Corregidora, Querétaro, C.P. 76920, Mexico*

[c] *Universidad Autónoma de Nuevo León, UANL, Facultad de Ciencias Químicas, DES Guerrero y Progreso S/N, Col. Treviño, Monterrey, NL, Mexico*

Received 17 October 2011; received in revised form 13 December 2011; accepted 15 December 2011

Available online 22 December 2011

Abstract

The $3CaO{\cdot}Al_2O_3$–Fe_2O_3 (C_3A–Fe_2O_3) system is important for the production of white clinker. In the present study this system was examined from the perspective of improving the sustainability of the production process. Microstructural evaluation was employed to explain the changes in color caused by variation of: iron content; temperature; type of atmosphere; and cooling conditions. It was found that color was more significantly affected by the iron content, temperature and type of atmosphere than by the type of cooling used. It was also observed that the utility of iron-rich raw materials could be maximized by understanding and enhancing the solubility of Fe_2O_3 in C_3A. It was found that a 2 wt.% Fe_2O_3 solid solution was stable only under kiln open to atmospheric conditions and remained clear at temperatures up to 1370 °C. However, the same 2 wt.% Fe_2O_3 solid solution suffered a significant change in color when the temperature rose to 1400 °C. Mössbauer spectroscopy showed that the oxidation state of Fe was Fe^{3+}, which did not change between 1370 and 1400 °C; however, a structural change in the C_3A–Fe_2O_3 solid solution was detected as a result of the alteration of the thermal treatment. The distinction between the structures at these two temperatures was that at 1370 °C, all of the Fe^{3+} had a tetrahedral coordination, while at 1400 °C, 19 wt.% of the Fe^{3+} appeared in octahedral sites, a result that was corroborated by Rietveld analysis.

Keywords: C. Color; D. Tricalcium aluminate; E. White clinker; E. Sustainability

1. Introduction

White Portland cement clinker (white clinker) is a material of technological interest, for which color control is crucial through the entire production process [1]. The degree of whiteness is carefully controlled in white cement production due to its use in architectonic applications where its color aesthetics are highly valued in the construction industry along with its efficient characteristics as a cementitious material. Unlike gray Portland cement clinker (gray clinker) in which iron is deliberately added as flux, the level of iron added during the production of white clinker is carefully controlled in order to produce a material which whiteness meets market requirements. Because of this constraint, white clinker production encounters greater sustainability and production challenges than those inherent to gray clinker production. Some of the main challenges to sustainability and production of white clinker are as follows:

1. The energetic demand for the production of white clinker is greater than the one needed to produce gray clinker. Gray clinker contains between 1 and 3 wt.% of Fe_2O_3, which favors an eutectic formation and, therefore, decreases the energetic demand of its production. On average, the energy to produce gray clinker in dry kilns with a preheater is in the range of 750–900 kcal/kg. In contrast, given the fact that the Fe_2O_3 content of white clinker is typically less than 0.5 wt.%, the energetic demand for its production is typically higher, ranging between 1400 and 1800 kcal/kg [2].

* Corresponding author. Tel.: +52 81 84002476; fax: +52 81 83760477.
E-mail address: lettorresg@yahoo.com (L.M. Torres-Martínez).

0272-8842/$36.00
doi:10.1016/j.ceramint.2011.12.032

2. The use of special raw materials with specific requirements for the production of white clinker involves their transportation from distant places to the cement plants. In contrast, the raw materials used in gray clinker production are commonly found near the cement plants, where the deposits are fully utilized. Because of the stringent limitations on iron content in white clinker production, the raw materials are processed in a highly selective fashion, producing a by-product of rejected material since it does not comply with stipulated quality control specifications. These two factors have the effect of making the white clinker sustainability deficit much larger than that of gray clinker production. Several researchers have tried to find a use for the raw material rejected to benefit from its iron content, using various physicochemical and microbiological methods [3–10]. However, although these options are technically feasible, they have not yet been embraced by the cement industry because of the additional costs incurred.
3. White clinker production requires a special bleaching process that is not required in gray clinker production which assures and increases clinker whiteness. Different methods have been developed for improving clinker whiteness, including the use of reducing atmospheres that can reduce Fe^{3+} to Fe^{2+}, which can substitute Ca^{2+} in the clinker phases diminishing the coloring power of Fe^{3+} [11,12] and the processes in which white clinker is obtained under a severe reducing atmosphere that reduces Fe^{3+} to metallic iron [13]. One of the ways in which a reducing atmosphere is generated is through the use of carbon or petcoke, which also contributes usable energy to the process [14]. Other process reported in the literature is the induction of a reducing atmosphere using waste raw materials contaminated with hydrocarbons, which has been reported as a way to obtain clinker with a very high whiteness [15]. The application of a reducing atmosphere in a section of the kiln and fast cooling that mainly uses water are two of the main techniques described in several patents that consider the goal of obtaining clinker of high whiteness [16–23]. The bleaching method most frequently used at the industrial level is a variant of fast clinker cooling, typically performed in the absence of oxygen. It is effective because the Fe^{2+} is locked into the glass phase of the clinker when it is fast cooled. Significant improvement of clinker whiteness has also been reported when fast cooling was carried out using either water or organic solvents such as ethylene glycol and triethanolamine [24].

On the other hand, it is well known that the $3CaO{\cdot}Al_2O_3$ (C_3A) phase has the capacity to form solid solutions of some of the impurities present in the clinker, such as Na_2O, K_2O, SiO_2, MgO and Fe_2O_3. Except for K_2O, the solid solutions result in an increase in the C_3A cell parameters. In the specific case of the Fe_2O_3 solid solution, some authors have reported a solid solution limit between 3 and 4 wt.% of Fe_2O_3 [25–31].

In addition to the capacity of C_3A to incorporate Fe_2O_3 into its structure, the present work also focuses on the study of the effects of different synthesis conditions, specifically the kiln oxygen atmosphere, type of cooling and temperature (in the range between 1300 and 1450 °C). This work originated from the need to apply new analysis techniques to understand the role of iron in the coloring of white clinker and, at the same time, to contribute to the understanding of the level of importance of the factors that could allow the future production of white clinker using rejected raw materials with a high content of iron, which at the present is not feasible.

2. Materials and methods

2.1. Synthesis conditions

Samples were synthesized under two different sets of conditions, which are described in the following two experimental schemes.

In scheme I (shown in Fig. 1) the C_3A phase was synthesized with an Fe_2O_3 content of 0, 1, 2, 3, 4 and 6 wt.% at a constant temperature of 1370 °C. The C_3A phases containing each Fe_2O_3 concentration were synthesized under two oxygen kiln conditions (an oxygen-depleted atmosphere and a kiln open to atmospheric conditions) and under two cooling conditions (slow cooling inside the deactivated kiln and fast cooling by quenching in water). A total of 24 samples were synthesized during experimentation on scheme I. Specifically for the 0 and 2 wt.% Fe_2O_3 samples, a 2^f experimental design was set, where the two factors studied were the two levels of Fe_2O_3 concentrations and the two levels of oxygen kiln conditions, and the response variable was the degree of color of the samples after their synthesis at 1370 °C. The importance of using a 2^f experimental design was to detect interactions between the two factors studied. The results of the 2^f were analyzed using the Minitab 15 experimental design software.

In scheme II (shown in Fig. 2), the C_3A phase with an Fe_2O_3 content ranging from 0, 1, 2, 3, 4 and 6 wt.% was synthesized exclusively under a kiln open to atmospheric conditions. Two different cooling conditions and five synthesis temperatures

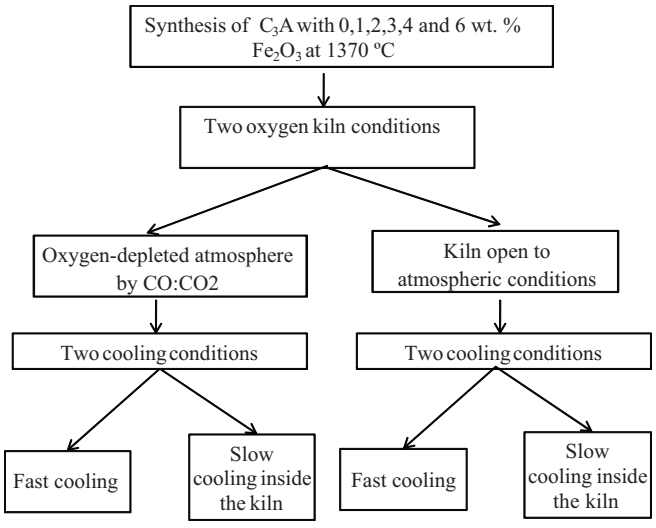

Fig. 1. Experimental scheme I.

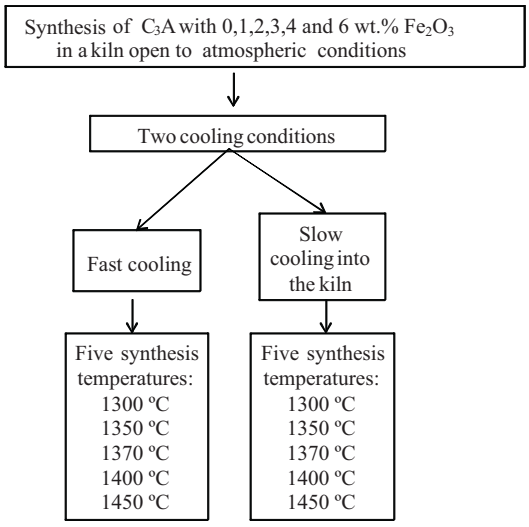

Fig. 2. Experimental scheme II.

(1300, 1350, 1370, 1400 and 1450 °C) were used. A total of 60 different samples were synthesized during experimentation on scheme II.

Tablets with a mass of 1.5 g were made using a stoichiometric mixture of $CaCO_3$ (Fermont) and Al_2O_3 (Aldrich) for experimental schemes I and II. The appropriate amount of Fe_2O_3 (Aldrich) was added in each non-zero case. All reagents used in this research were of analytical grade. The tablets were prepared by pressing the powder mixture at 3800 kg/cm^2 for 5 min.

Samples for both phases were synthesized in a Lindberg Model 54233 lab tubular kiln. After testing with a large number of temperatures and residence times, it was defined that the most suitable synthesis conditions for scheme I consisted of a residence time of 10 h and a temperature of 1370 °C. Under these conditions, it was possible to obtain a C_3A phase containing an amount of free lime close to 1% in both atmospheres using a single step synthesis without intermediate grinding (see Fig. 3). Every thermal process included a decarbonation step, which was carried out at 900 °C for 30 min. The oxygen-depleted atmosphere was induced by passing a 60 cc/min flow of a 1:1 mixture of CO_2 and CO through the alumina tube for the entire thermal treatment. When the oxygen-depleted atmosphere was used, a concentration of 0% was detected by direct measurement. When the kiln was open to atmospheric conditions, the extreme edges of the alumina tube were left open to the outside environment. However, the edges were covered by a permeable ceramic fiber to avoid drastic changes in the temperature profile inside the tubular kiln.

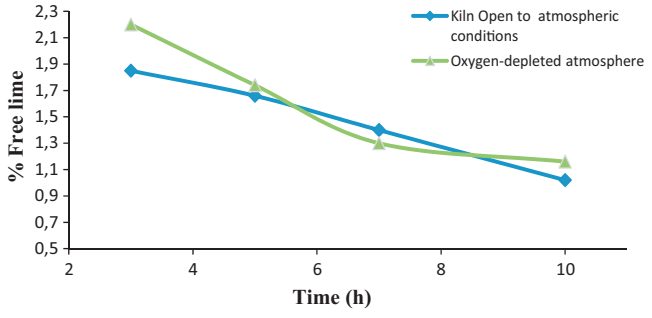

Fig. 3. Percentage of free lime in samples synthesized under a kiln open to atmospheric conditions and to oxygen-depleted atmosphere at 1370 °C.

2.2. Sample characterization

The samples were characterized by powder X-ray diffraction analysis using a Siemens D 5000 diffractometer, which used Cu radiation ($\lambda = 1.5418$ Å) and a graphite monochromator. The acceleration potential and tube current were 35 kV and 25 mA, respectively. Routine analysis were carried out using an irradiation time of 1.0 s, a step size of 0.05° in 2θ and a sample holder velocity of 15 rpm. Scanning was carried out in the diffraction range from 5 to 90° of 2θ to determinate if the phase of interest was present. In addition, the cell parameters were determined by an internal standard method in which the sample was mixed with 10 wt.% of KCl. A 6-s step time was used for each 0.01° step in the cell parameter analysis.

Sample color was determined with a CIEL*a*b* system with a GretagMacbeth Color Eye 9000A Spectrophotometer using the D65 illuminant and a viewing angle of 10°. The measurement was performed by placing the tablet directly on the window of the spectrophotometer.

To identify the possible formation of new colored compounds rich in iron and not detected by XRD, six samples were analyzed by Transmission Electron Microscopy (TEM). A Jeol instrument (model JEM-2010) working at 200 kV was used for this purpose.

Finally, two samples from scheme II, both containing 2 wt.% of Fe_2O_3 and obtained at 1370 °C and 1400 °C, were characterized by Mössbauer spectroscopy. Measurements by Mössbauer spectroscopy were carried out by transmission at a constant acceleration. The gamma radiation source was ^{57}Co(Rh), and the isomeric shifts (IS) were determined with respect to α-Fe at 77 K. Spectral numeric analysis was carried out by the MOSFIT software, which was developed by Teillet Varret from the Université Du Maine in France.

3. Results and discussion

3.1. Scheme I results

3.1.1. Color evaluation at first glance

The samples obtained by the different synthesis conditions used in scheme I are shown in Fig. 4. As Fig. 4 shows, there is substantial variation of color in the samples, ranging from white to very dark, including gray, brown, light brown and dark brown. The samples obtained in the oxygen-depleted atmosphere tended to be darker with less iron content than those obtained in a kiln open to atmospheric conditions. Samples with 1 wt.% of Fe_2O_3, regardless of the synthesis condition, were always clearer than the others. For samples with 2 wt.% of Fe_2O_3, there was a significant color difference between samples

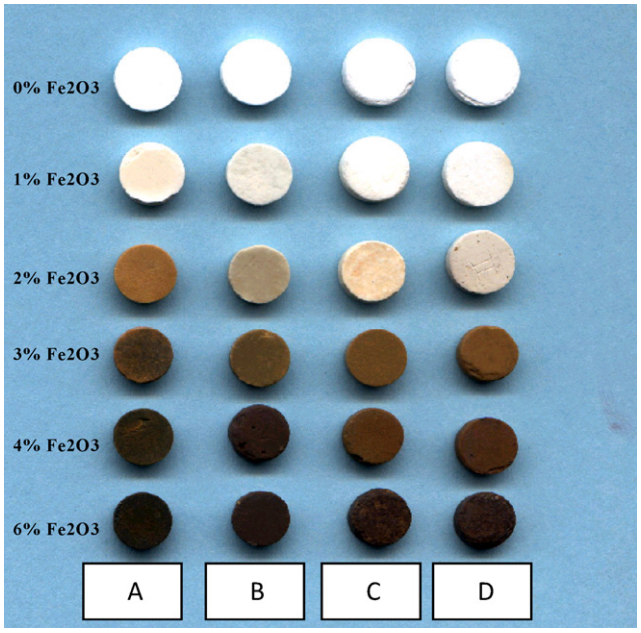

Fig. 4. Samples of the C_3A–Fe_2O_3 system obtained under two types of atmosphere and cooling conditions. Column A: oxygen-depleted atmosphere; fast cooling, column B: oxygen-depleted atmosphere; slow cooling, column C: kiln open to atmospheric conditions; fast cooling, column D: kiln open to atmospheric conditions; slow cooling.

obtained in different atmospheric conditions; the samples obtained in open to atmospheric conditions were clearer than those obtained in an oxygen-depleted atmosphere. In general, throughout the testing series, samples obtained under an oxygen-depleted atmosphere that contain *X*% Fe_2O_3 tended consistently to have similar coloration to samples obtained under open to atmospheric conditions with *X* + 1% Fe_2O_3.

3.1.2. Color measurement by spectrophotometry

Table 1 shows the color parameters *L**, *a** and *b** as a function of the Fe_2O_3 content of samples obtained under both atmospheres. The type of atmosphere had a greater influence on the color than the cooling process used, particularly on samples with approximately 2 wt.% Fe_2O_3. In this case, while the samples obtained in a kiln open to atmospheric conditions had an *L** value of approximately 80, the samples obtained under the oxygen-depleted atmosphere had an *L** value of approximately 50.

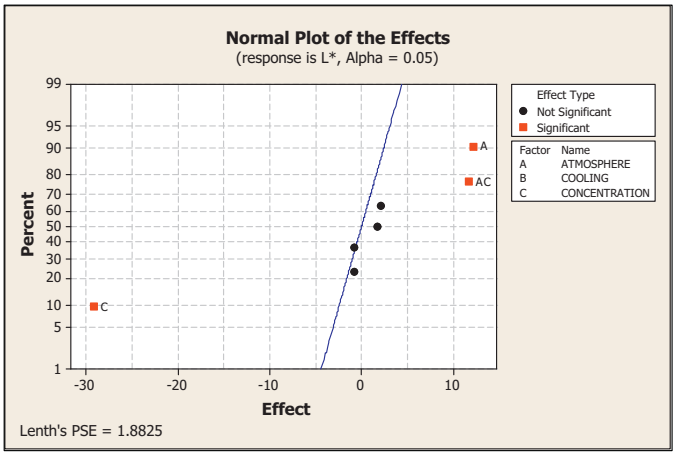

Fig. 5. 2^f DOE 0–2 wt.% Fe_2O_3, normal plot of the effects.

3.1.3. 2^f design of experiments (DOE) comparing the color of C_3A samples without Fe_2O_3 and with 2 wt.% of Fe_2O_3, under two types of atmosphere at 1370 °C

The results of the 2^f DOE indicated that the color difference between samples with 0 and 2 wt.% of Fe_2O_3 under two levels of oxygen kiln conditions is significantly influenced by these three main factors: (1) the Fe_2O_3 concentration, (2) the type of atmosphere used during the synthesis and (3) the interaction between the last two factors, as indicated by the Normal Plot of the effects in Fig. 5. According to the DOE, the whiteness of the pure C_3A phase was diminished significantly by the introduction of 2 wt.% of Fe_2O_3 (single factor) as well as by the use of the oxygen-depleted atmosphere (single factor). However, the interaction between the Fe_2O_3 content and the type of atmosphere (interaction between two factors) indicated that a significant increase in whiteness occurred when a clinker with 2 wt.% of Fe_2O_3 was synthesized under a kiln open to atmospheric conditions compared with the production of an equivalent sample in an oxygen-depleted atmosphere.

Fig. 6 shows a three-dimensional color graph in which the variation of the parameter *L** as a function of the Fe_2O_3 content and the cooling rate can be observed. The effect of oxygen-depleted atmosphere on the coloration of samples with 2 wt.% of Fe_2O_3 is highly visible. In samples obtained in a kiln open to atmospheric conditions, a substantial color change occurs as the Fe_2O_3 content increases from 2 to 3 wt.%. Compared with the effects of the iron content and the type of atmosphere, the type

Table 1
Colorimetric parameters for samples obtained at 1370 °C.

Fe_2O_3 (wt.%)	Kiln open to atmospheric conditions, slow cooling			Kiln open to atmospheric conditions, fast cooling			Oxygen-depleted atmosphere, slow cooling			Oxygen-depleted atmosphere, fast cooling		
	*L**	*a**	*b**	*L**	*a**	*b**	*L**	*a**	*b**	*L**	*a**	*b**
0	99.66	−1.04	1.52	96.97	−1.10	2.08	96.51	−0.83	0.73	96.15	−1.43	1.94
1	90.88	−1.05	5.80	92.74	−1.11	7.18	85.51	−1.36	8.82	86.27	−0.98	11.45
2	78.24	0.56	12.15	80.56	0.40	14.00	58.10	0.21	17.95	52.72	3.77	23.42
3	48.18	4.29	19.79	48.68	2.44	18.02	36.15	2.02	13.83	31.02	−0.02	9.73
4	36.69	5.65	12.63	39.45	4.05	14.77	31.24	2.42	8.76	28.09	0.84	5.96
6	27.80	3.96	6.28	32.19	3.40	6.65	27.62	3.30	6.25	27.42	2.40	6.10

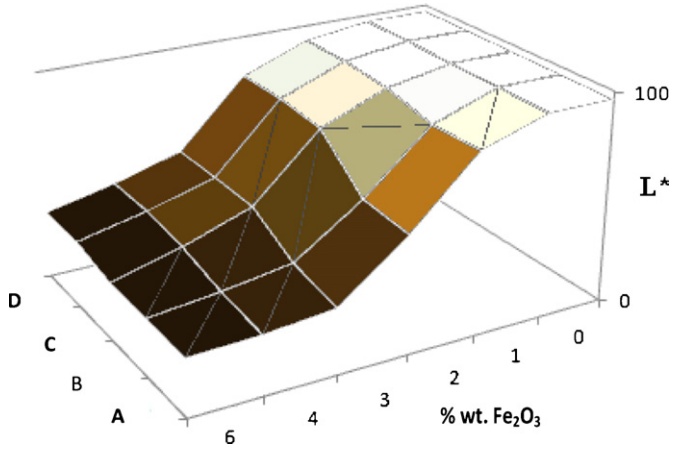

Fig. 6. Three-dimensional color graph, showing the variation of L^* with the Fe_2O_3 content, the atmosphere and the cooling rate. Column A: oxygen-depleted atmosphere; fast cooling, column B: oxygen-depleted atmosphere; slow cooling, column C: kiln open to atmospheric conditions; fast cooling, column D: kiln open to atmospheric conditions; slow cooling.

of cooling had a negligible effect on the color of the samples, as determined by the DOE.

3.1.4. Phases found by XRD in samples synthesized at 1370 °C

Fig. 7 shows three dimensional color graphs of the phases found in XRD as a function of the synthesis conditions. In the samples containing 0, 1 and 2 wt.% of Fe_2O_3, only the cubic phase of C_3A was found by XRD (JCPDF 70-0839). In the samples containing 3 wt.% or more of Fe_2O_3, the phase $Ca_3Al_{1.38}Fe_{0.62}O_5$ (JCPDF 420-1469) was found in addition to the C_3A phase. The color of the $Ca_3Al_{1.38}Fe_{0.62}O_5$ phase varies from yellow to brown, while the color of the C_3A phase is white. This phase-dependent color difference could explain the coloration acquired by samples with Fe_2O_3 content of 3 wt.% or greater. The iron-rich phases determined by XRD were the

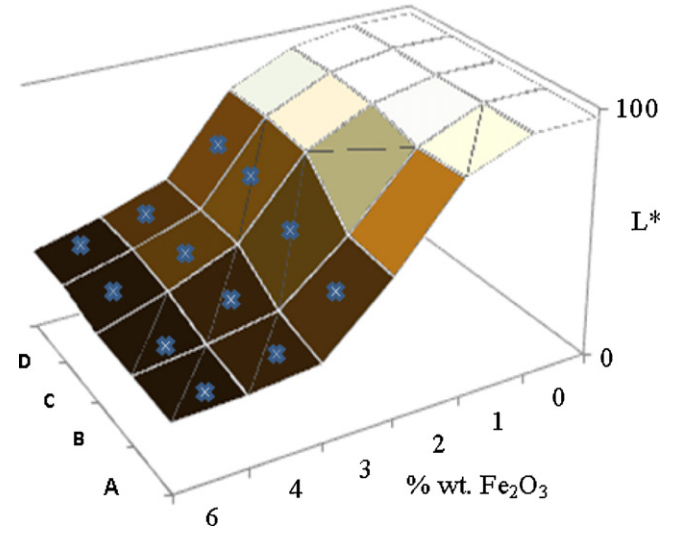

Fig. 7. Three-dimensional color graphs showing the crystalline phases found, (*x*) represents the additional phase $Ca_2Al_{1.38}Fe_{0.62}O_5$ determinate by XRD.

Table 2
Summary of crystalline phases determinate by TEM.

Fe_2O_3 (wt.%)	Kiln open to atmospheric conditions: fast cooling	Oxygen-depleted atmosphere: fast cooling
2	Fe_2O_3	$AlFeO_3$ orthorhombic and $AlFeO_3$ hexagonal
4	$AlFeO_3$ orthorhombic	$AlFeO_3$ orthorhombic
6	$AlFeO_3$ orthorhombic	$AlFeO_3$ orthorhombic

same for samples obtained under different atmospheres and cooling rates.

3.1.5. Phases found by TEM in samples synthesized at 1370 °C and fast cooled

TEM analysis was carried out to investigate the significant difference in color between samples containing 2 wt.% of Fe_2O_3 that were obtained under an oxygen-depleted atmosphere and a kiln open to atmospheric conditions. This analysis was performed with the purpose of finding iron-rich phases not detected by XRD. A total of six samples were analyzed by TEM, and their Fe_2O_3 contents were 2, 4 and 6 wt.%, with two samples for each atmosphere used, all of which were cooled by quenching in water. Fig. 8 shows TEM micrographs and diffraction patterns of these samples. In the C_3A sample containing 2 wt.% Fe_2O_3 and synthesized in a kiln open to atmospheric conditions, the only phase found corresponded to Fe_2O_3, indicating that some traces of the iron oxide used as a raw material did not react during the thermal treatment. In the C_3A sample with 2 wt.% Fe_2O_3 obtained in an oxygen-depleted atmosphere, the orthorhombic and hexagonal polymorphs of the $AlFeO_3$ phase were found. Table 2 shows a summary of the iron phases detected by TEM. Because the color of the orthorhombic and hexagonal $AlFeO_3$ phases ranged from gray to brown, their presence could explain the early coloration obtained in the C_3A sample with 2 wt.% of Fe_2O_3 under an oxygen-depleted atmosphere. In contrast, the dark color of the samples containing greater than 3 wt.% of Fe_2O_3 could be a result of the presence of both colored phases, $AlFeO_3$ and $Ca_3Al_{1.38}Fe_{0.62}O_5$. The orthorhombic $AlFeO_3$ phase seems to be the most stable phase because it is present in samples with 4 and 6 wt.% of Fe_2O_3 obtained under both atmospheric conditions; in contrast, the hexagonal phase only appears in samples obtained in an oxygen-depleted atmosphere with an Fe_2O_3 content of 2 wt.%.

3.1.6. Formation of solid solution in the C_3A–Fe_2O_3 system in the kiln open to atmospheric conditions

To provide a structural explanation for the difference in the color of the C_3A samples containing 2 wt.% of Fe_2O_3 as a result of the type of atmosphere used during their synthesis, a refinement of the cell parameters was carried out using the GSAS (General Structure Analysis System, 2004) software. Samples obtained in an open atmosphere showed a growth in their cell size as their Fe_2O_3 content increased, indicating that a solid solution was formed. In contrast, the cell size of samples synthesized in an oxygen-depleted atmosphere always kept the

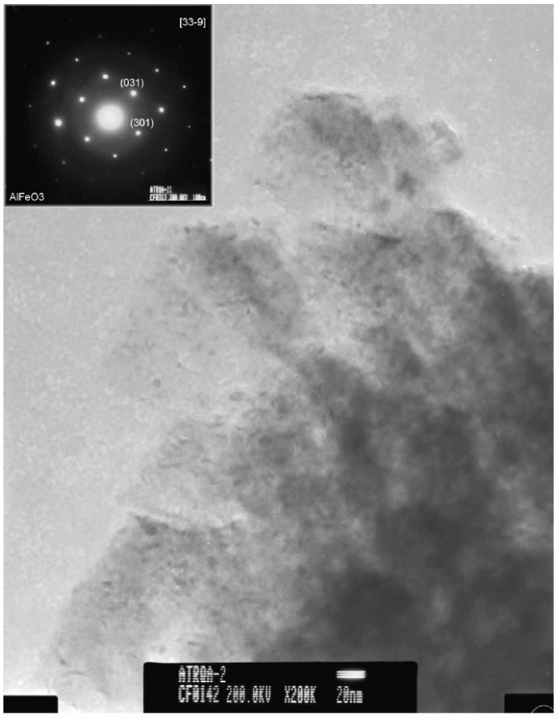

$AlFeO_3$ Hexagonal

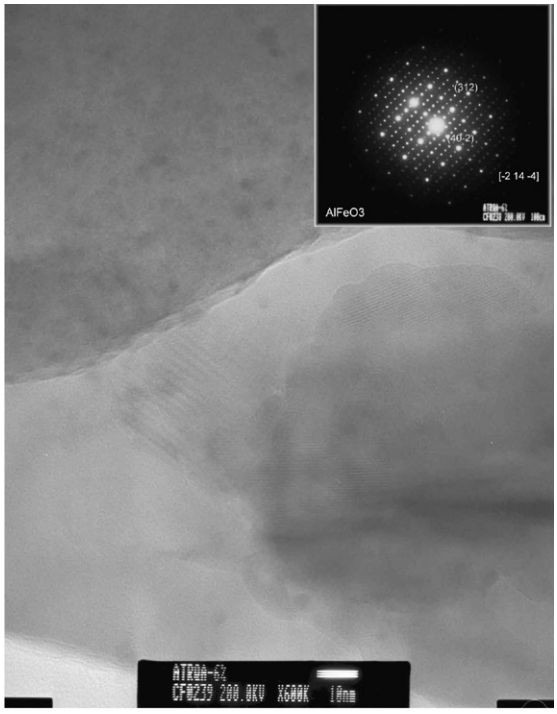

$AlFeO_3$ Orthorhombic

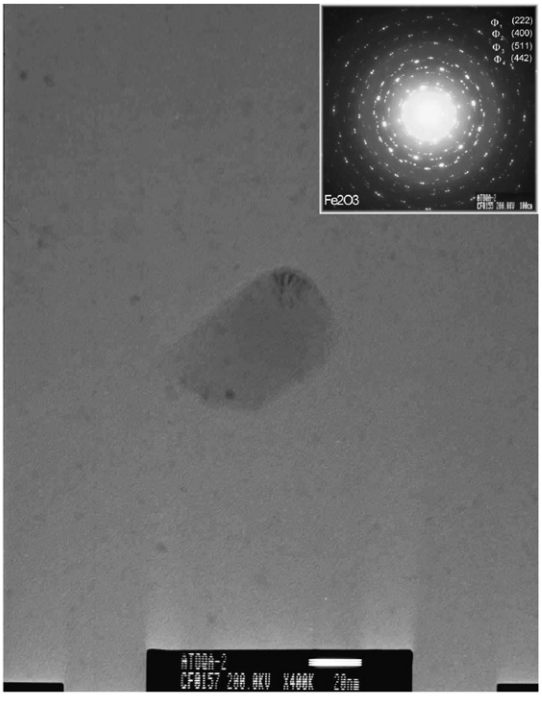

Fe_2O_3

Fig. 8. Micrographs and diffraction patterns obtained by TEM.

same size, independent of iron content, indicating that in this case, a solid solution was not formed (see Fig. 9).

According to Fig. 9, it is possible to introduce up to 2 wt.% of Fe_2O_3 into the C_3A structure; being this percentage of Fe_2O_3 lower than the amount reported in other works, which state values of 3 and 4 wt.% of Fe_2O_3 [29,30]. Therefore, the higher value of L^* in samples obtained in a kiln open to atmospheric conditions in the vicinity of 2 wt.% Fe_2O_3, can be explained by the formation of a solid solution between C_3A and Fe_2O_3. Solution formation does not occur when the samples are processed in an oxygen-depleted atmosphere, in which the colored $AlFeO_3$ phase is obtained instead of a solid solution.

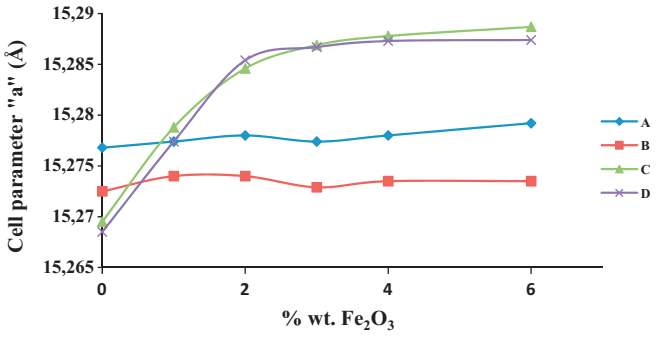

Fig. 9. Cell parameter "*a*" for samples with different Fe_2O_3 content obtained in different synthesis conditions at 1370 °C.

The failure to obtain a solid solution of C_3A–2 wt.% of Fe_2O_3 in an oxygen-depleted atmosphere may be explained by a change in the oxidation state of the iron. However, the analysis of this possibility was beyond the scope of this work.

In the present study, a value from 15.2685 Å to 15.2768 Å was obtained for the cell parameter "*a*" of the pure C_3A. This value differed from the reference value of 15.2631 Å. Although the difference is small, it could be attributed to the synthesis method used in this work, where intermediate grindings were not used, and the free lime content of approximately 1% was allowed to maintain a constant atmospheric type throughout the synthesis process and closely imitate the industrial process of clinker manufacturing. However, the value of the cell parameter "*a*" for the pure C_3A phase obtained under the different atmospheric conditions and cooling rates used in this work is very similar to that obtained in other works, in which the "*a*" value ranged from 15.26 to 15.27 Å [25,28–31].

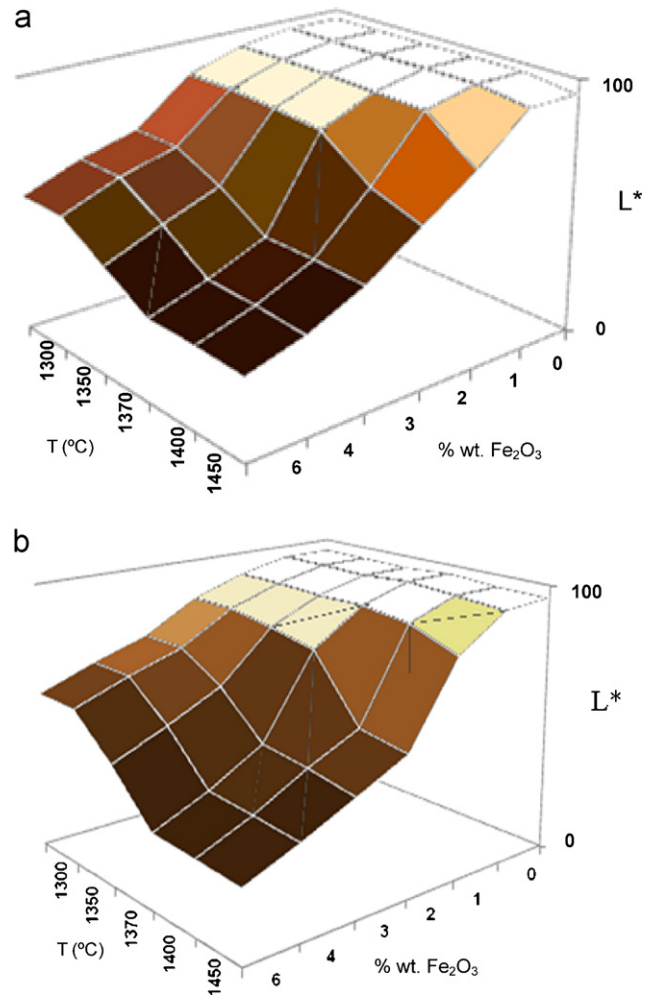

Fig. 10. Graphs showing the color variation and the L^* parameter as a function of the Fe_2O_3 content and the temperature for samples synthesized in a kiln open to atmospheric conditions: fast cooling (a) and slow cooling at 1370 °C (b).

3.2. Scheme II results

3.2.1. Color behavior with the temperature in the C_3A–Fe_2O_3 system

The scheme II results are shown in Fig. 10a and b. These results indicate that temperature is another important factor in the coloration of the C_3A–Fe_2O_3 system. The samples with 2 wt.% of Fe_2O_3 remained clear up to a temperature of 1370 °C, but they acquired significant color when the temperature was increased to 1400 and 1450 °C, as can be seen in Table 3. A similar phenomenon occurred in the samples with 1 wt.% of Fe_2O_3 when the temperature increased from 1400 to 1450 °C; however, this study focused on samples with 2 wt.% of Fe_2O_3 since it has a greater technological interest. In Fig. 11, a large color difference can be observed in the same sample with an increase in synthesis temperature of only 30 °C.

3.2.2. Changes in cell parameter "a" determined by XRD

The cell parameter "*a*" was affected by the change in temperature (see Fig. 12). When the temperature was increased from 1370 to 1400 °C, a decrease in the cell size occurred for samples containing 2 wt.% of Fe_2O_3. This change may be similar to the structural changes that occurred when the temperature was raised.

3.2.3. Mössbauer spectroscopy

Mössbauer spectroscopy was used to investigate the mechanics of the color change that occurs for samples with 2 wt.% of Fe_2O_3 when the synthesis temperature increases from

Table 3
Color parameters for samples obtained at different temperatures in samples with 2 wt.% of Fe_2O_3.

Synthesis condition	Temperature (°C)	L^*	a^*	b^*
Kiln open to atmospheric conditions: slow cooling.	1300	84.55	0.11	9.31
	1350	81.75	0.02	10.26
	1370	78.24	0.56	12.15
	1400	55.04	3.72	23.88
	1450	52.24	4.85	23.5
Kiln open to atmospheric conditions: fast cooling.	1300	86.26	1.43	10.8
	1350	84.95	1.22	12.66
	1370	80.56	0.4	14
	1400	52.46	5.61	22.73
	1450	48.97	7.4	21.25

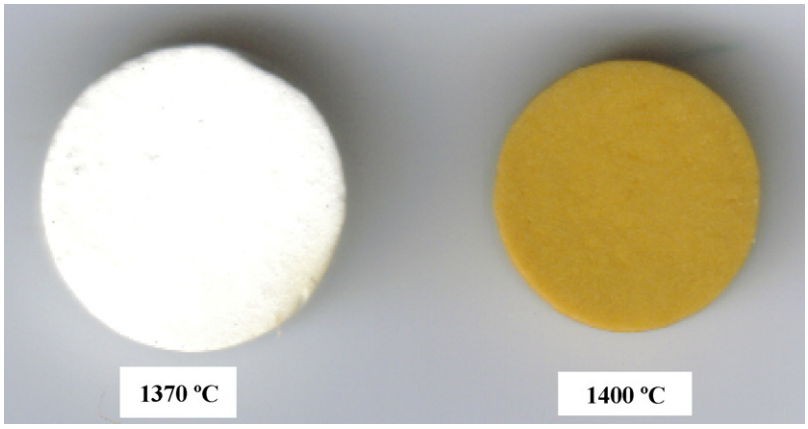

Fig. 11. Change of color in a sample with 2 wt.% of Fe_2O_3 when thermal treatment is increased from 1370 °C to 1400 °C.

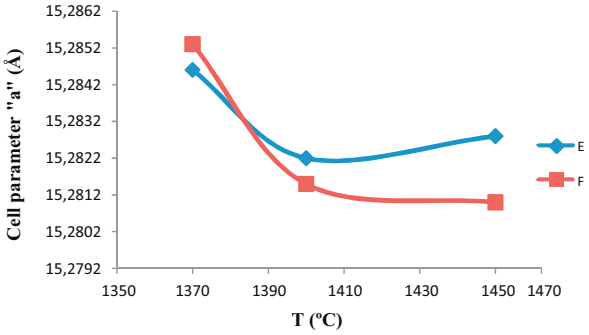

Fig. 12. Variation of the cell parameter "*a*" with the temperature for a sample with 2 wt.% of Fe_2O_3 synthesized in a kiln open to atmospheric conditions with fast cooling (E) and slow cooling (F).

1370 to 1400 °C. In detail, the technique was used to examine the dependence of the color change on changes in either the coordination number or the oxidation state of Fe. Two samples were studied with this technique, both of which were synthesized in a kiln open to atmospheric conditions and cooled slowly. The first sample was thermally treated at 1370 °C and the second one at 1400 °C. Mössbauer spectra are shown in Fig. 13, and the hyperfine parameters are shown in Table 4. According to Table 4, all of the Fe present in both samples is Fe^{3+}, however, a structural change occurs when the samples are heated from 1370 to 1400 °C. At 1370 °C, all of the Fe has a tetrahedral coordination, but at 1400 °C, 19% of the Fe has an octahedral coordination.

3.2.4. *Rietveld refinement*

Rietveld refinement was carried out on the phases obtained at 1370 and 1400 °C under an open atmosphere in an attempt to analyze structural changes and relate them to the color of the clinker. The C_3A structure was used as the basis for refinement, but Fe was allowed to occupy different positions (tetrahedral (Al^{3+}) and octahedral (Ca^{2+})), following the results obtained by Mössbauer spectroscopy. The analysis of C_3A obtained at 1370 °C shows occupation of Al^{3+} sites by 13% of Fe^{3+} ions and no occupation of octahedral positions. This occupation is approximately equivalent to a 4% mass fraction expressed as Fe_2O_3, which is close to the actual distribution. The occupation of two Al^{3+} positions by Fe^{3+} ions produces a tetrahedral environment with a coordination number of 4 O^{2-} ions, while octahedral sites are not occupied. This model is in complete agreement with the results of Mössbauer spectroscopy. However, the proportion of Fe^{3+} tetrahedral becomes 90:10.

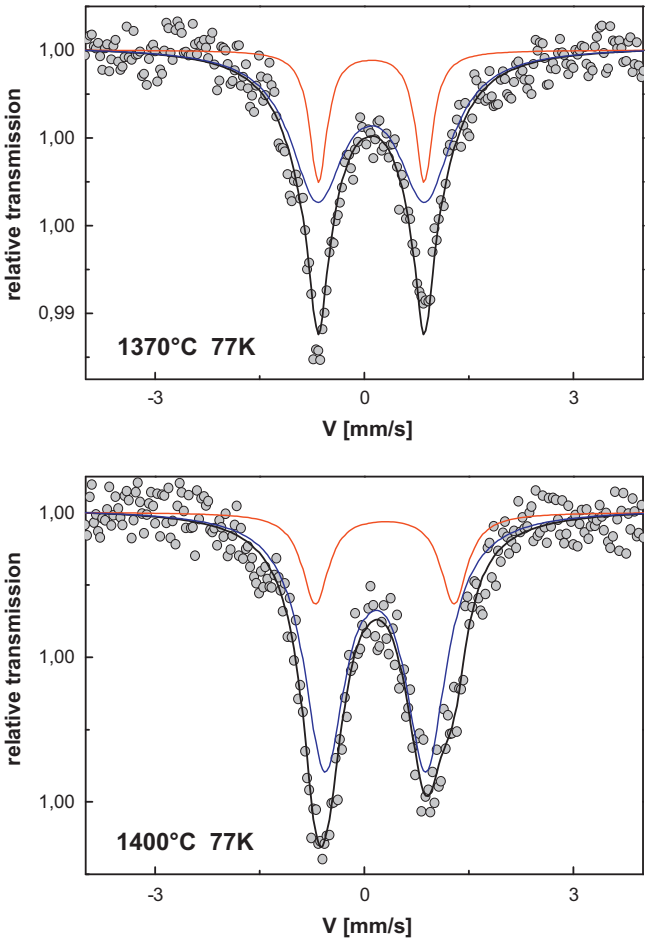

Fig. 13. Mössbauer spectra for samples with 2 wt.% of Fe_2O_3 obtained at 1370 °C and 1400 °C.

Table 4
Mössbauer parameters.

2 wt.% Fe_2O_3, kiln open to atmospheric conditions, slow cooling	Isomer shifts (IS)	Quadrupole splitting (QS)	Specie	%
1370 °C	0.25	1.48	Fe^{3+} (Tetra)	23
	0.24	1.51	Fe^{3+} (Tetra)	77
1400 °C	0.30	1.42	Fe^{3+} (Tetra)	81
	0.43	1.96	Fe^{3+} (Octa)	19

Table 5
Structural parameters obtained by Rietveld refinement.

Phase	C_3A at 1370 °C				C_3A at 1400 °C			
	Cell parameter: 15.285359 Å				Cell parameter: 15.281581 Å			
	$R_p = 5.74$, $R_{wp} = 7.34$, $R_2^f = 8.48$				$R_p = 5.99$, $R_{wp} = 7.34$, $R_2^f = 8.37$			
	X	y	z	Fraction	x	Y	Z	Fraction
Ca1	0	0	0	1.0	0	0	0	1.0
Ca2	1/2	0	0	1.0	1/2	0	0	1.0
Ca3	0.25626	0.25626	0.25626	1.0	0.25634	0.25634	0.25634	0.80119
Fe1	–	–	–	0.0	0.25634	0.25634	0.25634	0.19881
Ca4	0.37262	0.37262	0.37262	1.0	0.62652	0.62652	0.62652	1.0
Ca5	0.13752	0.37555	0.12796	1.0	0.13574	0.37605	0.1293	1.0
Ca6	0.37624	0.38395	0.12001	1.0	0.37431	0.38295	0.11905	1.0
Al1	0.25226	0.01341	0.01772	0.87498	0.25268	0.01298	0.01687	0.9682
Fe2	0.25226	0.01341	0.01772	0.12502	0.25268	0.01298	0.01687	0.0318
Al2	0.24450	0.23632	0.00757	0.98518	0.24343	0.23575	0.0059	0.9743
Fe3	0.24450	0.23632	0.00757	0.01482	0.24343	0.23575	0.0059	0.0257
O1	0.27587	0.11968	0.0062	1.0	0.28076	0.12156	0.00648	1.0
O2	0.49237	0.12790	0.24967	1.0	0.49231	0.12337	0.24727	1.0
O3	0.25992	0.28756	0.09831	1.0	0.25922	0.28852	0.09544	1.0
O4	0.23061	0.40792	0.28964	1.0	0.23236	0.4080	0.28959	1.0
O5	0.35495	−0.03968	−0.02321	1.0	0.35561	−0.03933	−0.02116	1.0
O6	0.14613	−0.00444	−0.02893	1.0	0.15163	−0.00002	−0.03201	1.0

For the sample obtained at 1400 °C, the diffusion of Fe^{3+} ions from tetrahedral to octahedral sites is observed. In this case, Fe^{3+} ions distribute to three possible sites: an octahedral-coordinated site originally occupied by a Ca^{2+} ion and two tetrahedral-coordinated Al^{3+} positions. However, these two sites have similar bond distances, making their environments nearly identical. In Mössbauer spectroscopy, this arrangement could be observed as only one tetrahedral position and one octahedral position, corroborating the agreement of both techniques. In this sample, Fe^{3+} ions could group into $[FeO_4]^{-5}$ units adjacent to

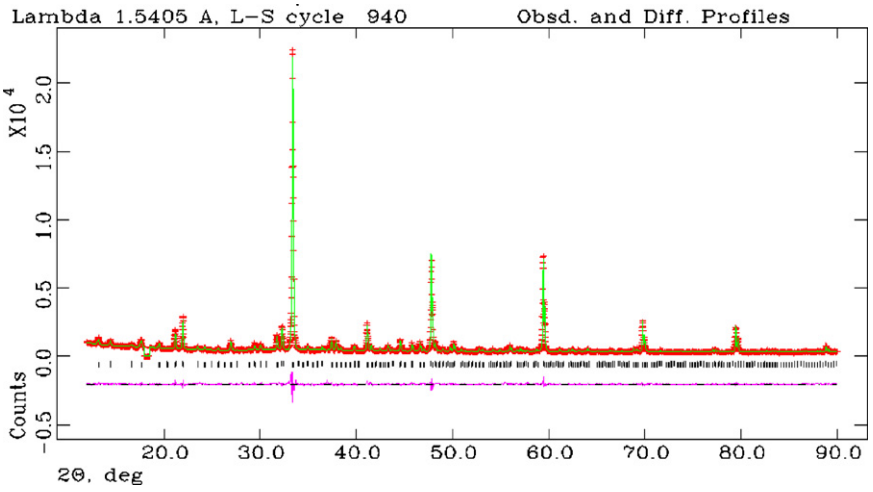

Fig. 14. Rietveld refinement graph of C_3A obtained at 1370 °C.

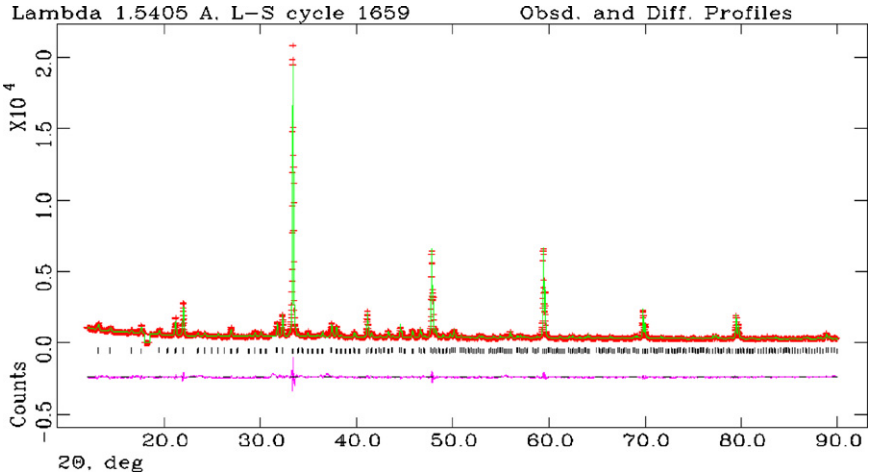

Fig. 15. Rietveld refinement graph of C_3A obtained at 1400 °C.

octahedral Fe^{3+} ions with possible delocalized electrons, producing the coloration observed in the C_3A phases. For the samples produced at 1370 °C, stretch paths do not allow the diffusion of Fe^{3+} and substitution of Ca^{2+}, however, for temperatures above 1400 °C diffusion was possible, affecting the average cell size and occupation in the octahedral and tetrahedral sites. Above 1400 °C the diffusion of Fe^{3+} was produced as a result of thermal vibration, as occurs in glass, aiding the migration of Fe^{3+} from easily available tetrahedral sites to more affordable octahedral sites, resulting in formation of color center defects [32]. Table 5 shows the structural parameters calculated by Rietveld refinement, and Figs. 14 and 15 show the Rietveld refinement graphs of the samples synthesized at 1370 and 1400 °C, respectively.

3.2.5. Model proposed to explain the color change

According to the results obtained by Mössbauer spectroscopy and corroborated by Rietveld refinement, the color change in the samples containing 2 wt.% of Fe_2O_3 that were heated from 1370 to 1400 °C can be attributed to possible electron delocalization caused by a structural change induced by the diffusion of Fe^{3+} ions from tetrahedral to octahedral sites in the C_3A structure. The two structures proposed are shown in Figs. 16 and 17.

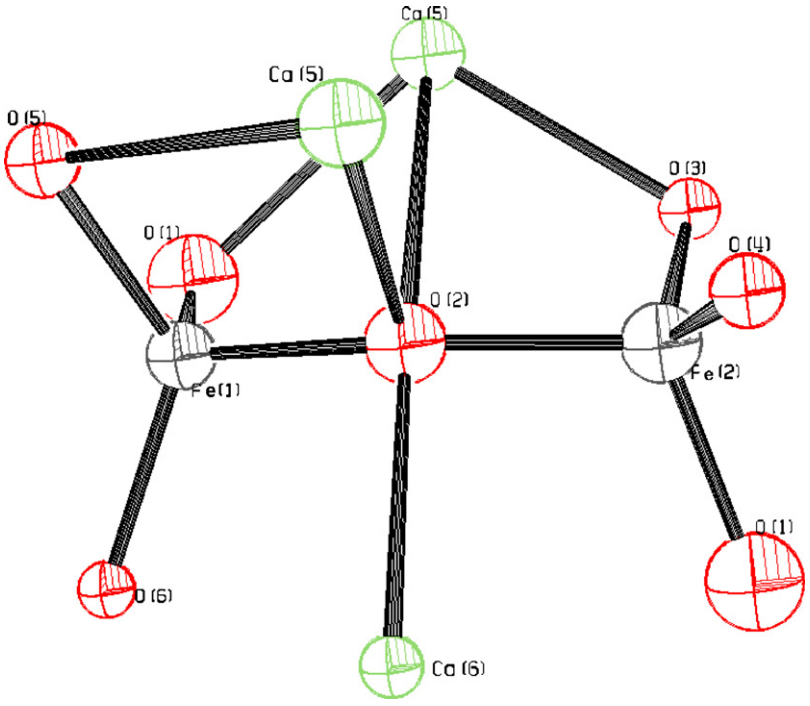

Fig. 16. Structural model of the solid solution C_3A–Fe_2O_3 at 1370 °C.

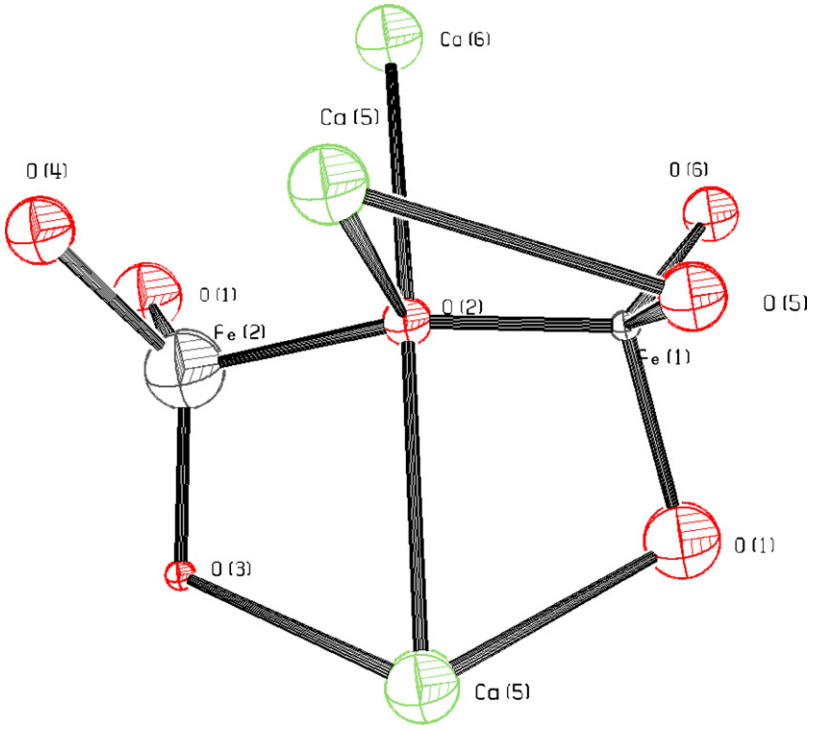

Fig. 17. Structural model of the solid solution C_3A–Fe_2O_3 at 1400 °C.

4. Conclusions

The color of samples of the C_3A–Fe_2O_3 system is affected by the Fe content as well as by the type of atmosphere and temperature of the synthesis. However, the type of cooling used had no observed effect. For the same Fe_2O_3 content, the samples obtained at 1370 °C in an oxygen-depleted atmosphere showed more coloration than samples obtained in a kiln open to atmospheric conditions. The clearer color of the samples synthesized in the kiln open to atmospheric conditions can be explained by the formation of a solid solution of C_3A–Fe_2O_3, which indicates an increase of the cell parameter "*a*". Under the experimental conditions of this paper, it was found that the solid solution has a limited solubility of approximately 2 wt.% Fe_2O_3 in a kiln open to atmospheric conditions. No evidence was found for the formation of a solid solution when the samples were obtained in an oxygen-depleted condition.

The samples obtained in a kiln open to atmospheric conditions remained clear with an Fe_2O_3 content as high as 2 wt.%, after which they acquired color because of the formation of colored phases such as $Ca_3Al_{1.38}Fe_{0.62}O_5$ and $AlFeO_3$. The samples synthesized in an oxygen-depleted atmosphere acquired color at 2 wt.% because there was no formation of a solid solution; therefore, the colored phases appeared earlier than during the synthesis open to the atmosphere.

Clear samples with 2 wt.% of Fe_2O_3 obtained in an open atmosphere at 1370 °C became colored when they were heated to 1400 °C as a result of a structural change in the C_3A–Fe_2O_3 solid solution. At 1370 °C, all the Fe had a tetrahedral coordination, but at 1400 °C 19% of the Fe migrated to octahedral sites. Despite the structural change, Mössbauer spectroscopy indicates that in these two samples, all of the iron was present as Fe^{3+}. Therefore, the change in color was not associated with a change in the oxidation state of the Fe. The Rietveld refinement results were in agreement with the structural change determined by Mössbauer spectroscopy.

Contrary to typical assumptions about the whitening of clinker, in the present work, neither the fast cooling by quenching in water nor an oxygen-depleted atmosphere improved the whiteness on the samples.

Finally, temperature was found to play an important role in the C_3A coloration phenomenon and possibly in the white clinker coloration process; therefore, it is recommended that the lowest temperature possible should be used in the manufacture of white clinker in order to improve its whiteness.

Acknowledgments

The authors want to thank Dr. Jean-Marc Greneche at the "Faculté des Sciences, Université du Maine" for his support performing and interpreting the Mössbauer spectroscopy results and Dr. Lorenzo Martínez at "Instituto de Ciencias Físicas" (UNAM) for his support in performing the TEM studies. The authors also want to thank CEMEX, PAICYT UANL 2010 and PROMEP/103.5/11/4330 for the financial support for this project.

References

[1] A. Virella, El color de los cementos, Cemento–Hormigón 423 (1969) 585–623.

[2] Cemex and Lafarge, personal communications.
[3] L. Toro, A. Paponetti, B. Passariello, Proceso Per la Rimozione del Ferro da Concentrati di Caolino, Quarzo ed Altri Materiali di Interese Industriale, Italian Patent No. 217070 A/90 (1990).
[4] F. Vázquez, L.M. Torres, L.L. Garza, A. Martínez, W. López, A Mexican kaolin deposit: XANES characterization, mineralogical phase analysis and applications,(Caracterización por XANES, análisis mineralógico y aplicación industrial de un depósito de caolín en México), Mater. Construcc. 59 (294) (2009) 113–121.
[5] M. Hosseini, Bioleaching of iron from highly contaminated kaolin clay by Aspergillus Niger, Appl. Clay Sci. 37 (3) (2007) 251–257.
[6] A. Newns, R. Pascoe, Influence of path length and slurry velocity on the removal of iron from kaolin using a high gradient magnetic separator, Miner. Eng. 15 (2002) 465–467.
[7] J. González, M. Ruiz, Bleaching of kaolins and clays by chlorination of iron and titanium, Appl. Clay Sci. 33 (2006) 219–229.
[8] P. Pinheiro, Beneficiation of a commercial kaolin from Mar de Espanha, Minas Gerais: Chemistry and Mineralogy, J. S. Am. Earth Sci. 20 (2005) 267–271.
[9] F. Veglio, B. Passariello, L. Toro, A. Marabini, Development of a bleaching process for a kaolin of industrial interest by oxalic, ascorbic, and sulfuric acids: preliminary study using statistical methods of experimental design, Ind. Eng. Chem. Res. 35 (1996) 1680–1687.
[10] V. Ambikadevi, M. Lalithambika, Effect of organic acid on ferric iron removal from iron-stained kaolinite, Appl. Clay Sci. 16 (2000) 133–145.
[11] A. Zubekhin, Composition and structure of the iron-containing phases of white Portland cement clinker, Tsement 10 (1982) 11–14.
[12] L. Kakurina, Study of white cements from low-temperature synthesis by the methods of electron paramagnetic resonance and optical spectroscopy, VINITI 15 (1982) 1785–1882.
[13] J. Rezola, Cemento Portland artificial blanco y sus aplicaciones, Instituto Eduardo Torroja de la Construcción y del Cemento, Madrid, 1975pp. 92–96.
[14] Ma. Xiotao, The test on firing of white cement clinker using mixed fuel of oil and coal, Proc. Beiging Int. Symp. Cem. Concr. 1 (1993) 509–510.
[15] P. Gaidzhurov, Effect of organic impurities on sintering and properties of clinker of white Portland cement, Khim. Tecknol. 31 (7) (1988) 72–75.
[16] G. Koeberer, et al., Krupp Fordertechnik GmbH, US Patent 56,18,104 (April 8, 1997).
[17] T. Ichiyanagi, et al., Kabushiki Kaisha, US Patent 47,17,337 (January 5, 1988).
[18] J. Pons de Vinals, Valenciana de Cementos Portland S.A., US Patent 47,67,462 (August 30, 1988).
[19] S.M. Cohen, Fuller Company, US Patent 46,82,948 (July 28, 1987).
[20] T. Itoh, et al., Ricoh Company Ltd., US Patent 45,95,948 (June 17, 1986).
[21] T. Ichiyanagi, et al., Chichibu Cement Kabushiki Kaisha, US Patent 45,73,908 (March 4, 1986).
[22] P. Weber, Krupp Polsisu AG, US Patent 45,60,412 (December 24, 1985).
[23] G. Roth, et al., BKMI Industrieanlagen GmbH, US Patent 44,61,645 (July 24, 1984).
[24] I. Teoreanu, Correlations between the cooling and the properties of white Portland cement clinker, Mater. Constr. (Bucharest) 19 (1) (1989) 15–19.
[25] S. Dietmar, Influence of Cr, Ni, and Zn on the properties of pure clinker phases. Part II. C_3A and C_4AF, Cement Concrete Res. 29 (1999) 651–657.
[26] L. Gobbo, C_3A polymorphs related to industrial clinker alkalies content, Cement Concrete Res. 34 (2004) 657–664.
[27] B.M. Mohamed, Kinetics and mechanism of formation of tricalcium aluminate, $Ca_3Al_2O_6$, Thermochim. Acta 388 (2002) 105–114.
[28] A.K. Prodjosantoso, B.J. Kennedy, Heavy metals in cement phases: on the solubility of Mg, Cd, Pb and Ba in $Ca_3Al_2O_6$, Cement Concrete Res. 33 (2003) 1077–1084.
[29] S. Dietmar, Crystal structure refinement and hydration behavior of doped tricalcium aluminate, Cement Concrete Res. 36 (2006) 2011–2020.
[30] M. Hassaan, M. El-Desoky, Y. Abou Zeid, Estimation of the solubility limit of iron in tricalcium aluminate using different techniques, Mater. Sci. Eng. AZ76 (2000) 147–151.
[31] A. Gaki, R. Chrysafi, G. Kakali, Chemical synthesis of hydraulic calcium aluminate compounds using the Pechini technique, J. Eur. Ceram. Soc. 27 (2007) 1781–1784.
[32] C.R. Kurkjian, Coordination of Fe^{3+} in glass, Phys. Chem. Glasses 9 (1968) 73–83.